AGU PUBLICATIONS

JGR

Journal of Geophysical Research: Space Physics

RESEARCH ARTICLE

10.1002/2014JA019921

Key Points:
- Heating by VLF transmitters affects the signal above the ionosphere by 1–2 dB
- Heating by lightning affects the signal above the ionosphere by 10 dB or more
- In different scenarios the signal can be enhanced or attenuated by heating

Correspondence to:
R. A. Marshall,
ram80@stanford.edu

Citation:
Marshall, R. A. (2014), Effect of self-absorption on attenuation of lightning and transmitter signals in the lower ionosphere, *J. Geophys. Res. Space Physics*, *119*, doi:10.1002/2014JA019921.

Received 25 FEB 2014
Accepted 25 APR 2014
Accepted article online 29 APR 2014

Effect of self-absorption on attenuation of lightning and transmitter signals in the lower ionosphere

R. A. Marshall[1]

[1] Department of Aeronautics and Astronautics, Stanford University, Stanford, California, USA

Abstract The attenuation of VLF signals from lightning and ground-based VLF transmitters during transionospheric propagation has been the subject of recent interest, as discrepancies have been found between satellite data and model calculations. Previous modeling efforts, however, have not considered the self-absorption effect due to nonlinear heating and ionization in the lower ionosphere. A self-consistent model of ionospheric heating is presented here using a time-domain model of VLF wave propagation through the ionosphere. The model is able to estimate the attenuation of signals due to heating below ~100 km altitude. In this model, the ionospheric state is updated as the fields propagate, leading to changes in collision frequency and electron density, which in turn affect the wave propagation. We use this model for ground-based VLF transmitters at different frequencies, amplitudes, and latitudes (i.e., magnetic dip angle), and for lightning-generated sferics with different amplitudes, at different latitudes, and using a variety of ionospheric density profiles. We find that the inclusion of self-consistent heating causes a change in the transionospherically propagating wave amplitude that varies considerably with the source amplitude and other parameters. Typical values for the heating contribution to wave attenuation are 1−2 dB for VLF transmitters, but greater than 10 dB for large amplitude lightning discharges. An interesting effect is observed for VLF transmitters and low-amplitude lightning, where the signal is actually enhanced due to heating, rather than attenuated, in the direction propagating across the Earth's magnetic field.

1. Introduction

High-power very low frequency (VLF) waves are generated primarily by lightning and by ground-based VLF transmitters. The VLF range is effective for long-range communication because most of the energy remains trapped between the conducting Earth and the lower ionosphere, forming the Earth-ionosphere waveguide. However, a significant fraction of the VLF wave energy leaks through the ionosphere and into the Earth's magnetosphere, where it propagates as whistler mode waves and affects the plasmasphere and radiation belts. These whistlers can induce pitch angle scattering and precipitation of trapped radiation belt electrons [e.g., *Imhof et al.*, 1983; *Inan and Carpenter*, 1987]. Whistlers launched by lightning discharges primarily interact with radiation belt electrons in the range of hundreds of keV up to 1 MeV. It has been shown [*Abel and Thorne*, 1998] that these whistlers play a significant role in maintaining the slot region between the inner and outer radiation belts. However, an accurate assessment of the effects of lightning on the radiation belts requires accurate measurement of the VLF wave amplitude injected into the magnetosphere.

While *Cohen et al.* [2012] and *Graf et al.* [2013a] estimate that ~20% of the VLF wave energy propagates into the magnetosphere, some fraction of this energy is lost to absorption in the lower ionosphere. Estimates of the absorption through the ionosphere were first presented by *Helliwell* [1965, Figure 3–35], and those estimates have been used by almost all studies since [e.g., *Abel and Thorne*, 1998; *Bortnik*, 2004; *Kulkarni et al.*, 2008; *Starks et al.*, 2008; *Golden et al.*, 2010]. Recent in situ satellite observations [*Starks et al.*, 2008] have questioned the validity of the *Helliwell* estimates, finding 20–40 dB discrepancy between these estimates and the satellite measurements.

Recent work has helped to close the discrepancy between satellite measurements and model estimates. *Cohen and Inan* [2012] used Detection of Electro-Magnetic Emissions Transmitted from Earthquake Regions (DEMETER) satellite data during passes over ground-based VLF transmitters to estimate the total power injected into the magnetosphere on a large statistical basis, both for daytime and nighttime. *Cohen et al.* [2012] compared these measurements to results of a full-wave method (FWM) [*Lehtinen and Inan*, 2008, 2009] model and found agreement to within ±6 dB, both for daytime and nighttime. *Graf et al.* [2013a] then used the FWM model to recompute transionospheric attenuation curves similar to those from

Helliwell [1965]. They again found agreement to within ±6 dB, and attributed the errors of previous comparisons to simplifying assumptions within the *Helliwell* formulation, in particular, the assumption of vertical incidence of the wave on the lower ionosphere. *Graf et al.* [2013b] then showed that the region of the ionosphere that is heated by ground-based VLF transmitters is much more extensive than previously though, extending thousands of kilometers laterally. For lightning, comparison between modeled wave amplitudes and measured amplitudes using the DEMETER satellite data is ongoing.

An effect that is not included in the recent FWM calculations is that of "self-absorption" of the VLF wave. When the VLF wave propagates through the ionosphere, it heats the collisional plasma, energy is lost to electron heating, and the wave is attenuated. However, the electron heating and (potentially) new ionization change the properties of the ionosphere, in particular, the electron-neutral collision frequency ν_{en} and (possibly) electron density N_e. These changing parameters in turn alter the propagation of the VLF wave. Accounting for these nonlinear effects may alter the estimates of absorption. In this paper, we estimate the contribution of self-absorption of the VLF wave for both transmitter and lightning-generated VLF signals.

2. Model

Because the full-wave method is inherently a frequency-domain solution, it cannot inherently account for self-absorption. Inclusion of this effect would require an iterative solution: the wave amplitude is estimated in the simulation space through the FWM model, and then heating and ionization are assessed from the steady state wave solution. The FWM could then be iterated on the modified ionosphere until it converges on a solution.

A simpler solution is to use a time-domain method that self-consistently updates the electron-neutral collision frequency and electron density during the wave propagation. Self-consistent models of the lightning-ionosphere interaction have existed for some time, beginning with the 1-D formulation of *Taranenko et al.* [1993a, 1993b]. Two-dimensional and 3-D models have been developed in recent years [*Cho and Rycroft*, 2001; *Nagano et al.*, 2003; *Marshall et al.*, 2010] and have assessed the chemical effects of lightning in the lower ionosphere through heating, ionization, optical emissions, dissociative attachment, and most recently, associative detachment [*Luque and Gordillo-Vázquez*, 2011; *Liu*, 2011; *Neubert et al.*, 2011].

In this paper we use the electromagnetic pulse (EMP) model of *Marshall* [2012] to calculate wave propagation and nonlinear effects due to lightning and VLF transmitters. The EMP model is a finite-difference time-domain (FDTD) model designed to simulate lightning discharges but is easily modified to simulate a sinusoidal source from a small dipole (similar to a ground-based VLF transmitter).

Details on the model formulation can be found in *Marshall* [2012]. Crucial to this application, the model is cast in spherical coordinates, which inherently accounts for Earth curvature. Arbitrary and inhomogeneous ionosphere, neutral atmosphere, magnetic fields, and ground parameters (conductivity and permittivity) can be included in the model.

We calculate nonlinear effects (heating and ionization) in the ionosphere differently for VLF transmitters and for lightning, for reasons that will be explained presently. For lightning, the electron mobility, ionization, attachment, and optical excitation rates are calculated as a function of electric field using BOLSIG+ [*Hagelaar and Pitchford*, 2005]; the detachment rate is calculated from equation (17) of *Neubert et al.* [2011]. Figure 1 of *Marshall* [2012] shows the rates used, which scale with neutral density, as a function of electric field. The electron mobility is then inversely related to the electron-neutral collision frequency by $\nu_{en} = q_e/(\mu_e m_e)$. The rates are precalculated using BOLSIG+ as a function of electric field and neutral density, so that application in the model is implemented with lookup table interpolation.

This method is perfectly valid for either VLF transmitters or lightning, as long as the electron distribution can be assumed to be stationary, which was shown to be true on time scales longer than ~2 μs by *Glukhov and Inan* [1996]; this is clearly valid for VLF transmitters operating in the tens of kHz and for most lightning sferics, which have measured rise times of 3–4 μs. However, in our method for calculating the electron mobility, which follows the method of *Pasko et al.* [1997], we threshold the mobility to a maximum value of $1.4856\,N/N_0$ m^2/V/s at low electric fields (modified slightly from the value in *Pasko et al.* [1997], thanks to updated calculations using BOLSIG+), in order to match the results of BOLSIG+ at higher field values to the maximum mobility at $E = 0$. This thresholding occurs for fields below $\sim 100\,N/N_0$ V/m, for which no change in mobility (heating) is calculated. For VLF transmitters, the field amplitude in the ionosphere falls

well below this threshold. As such, using the lightning model, no heating is calculated for VLF transmitters, while heating clearly does occur.

Instead, for VLF transmitters we use the heating method presented in *Rodriguez et al.* [1994] and *Graf et al.* [2013b], which updates the electron temperature due to heating, and also includes cooling:

$$\frac{3}{2}k_B N_e \frac{dT_e}{dt} = U - L_e \tag{1}$$

where $U = J \cdot E$ is simply Joule heating, which is trivial to calculate in the FDTD method. The term L_e is electron cooling, which includes empirical expressions for rotational, vibrational, and elastic transfer of energy from electrons to N_2 and O_2 as a function of T_e, T_0, N_e, N_{N_2}, and N_{O_2}; these expressions are listed in detail in *Graf et al.* [2013b]. In the time domain method, we discretize equation (1) above using a semiimplicit Euler method, which however does not guarantee stability.

From the electron temperature T_e, we calculate the updated collision frequency using the same method as *Rodriguez* [1994], derived by *Banks* [1966]. The collision frequency is calculated for electron-N_2 collisions and electron-O_2 collisions separately, and then the two rates are added:

$$\nu_{av}(e, N_2) = 2.33 \times 10^{-17} N_{N_2} (1 - 1.21 \times 10^{-4}\, T_e)\, T_e \tag{2a}$$

$$\nu_{av}(e, O_2) = 1.82 \times 10^{-16} N_{O_2} (1 + 0.036\, T_e^{1/2})\, T_e^{1/2} \tag{2b}$$

$$\nu_{en} = \nu_{av}(e, N_2) + \nu_{av}(e, O_2) \tag{2c}$$

The procedure for self-consistently updating the fields and heating is thus

1. E and B are updated using the standard FDTD algorithm;

2a. For lightning, (i) mobility, ionization, attachment, detachment, and optical excitation rates are updated at each grid point based on the local effective electric field; (ii) the electron-neutral collision frequency is calculated from electron mobility; and (iii) ionization, attachment, and detachment rates are used to update the electron density.

2b. For transmitters, (i) electron temperature is updated using the discretized version of equation (1) and equations for cooling; and (ii) collision frequency is updated from electron temperature using equations ((2a)–(2c));

3. Finally, the current J is updated according to the Langevin equation, using the method of *Lee and Kalluri* [1999], including a collisional term.

2.1. Comparison of Heating Methods

To verify the relative accuracy of the lightning and transmitter heating methods above, we use the transmitter heating method in a lightning simulation and compare the results for the updated collision frequency. First, we describe a few of the "default" parameters used.

For all simulations discussed in this paper, we use an International Reference Ionosphere (IRI) model [*Bilitza and Reinisch*, 2008], computed for 1 January 2011 at midnight local time, 40°N, 100°W. (Note that in this paper we restrict our investigation to nighttime propagation; the high electron density during daytime results in an extremely small time step in the FDTD method to maintain stability, rendering the problem intractable.) Mobility, detachment, attachment, ionization, and optical excitation rates all scale with neutral density, which is taken from an MSIS-E-00 profile [*Hedin*, 1991] at the same time and location. We use a magnetic field magnitude of 50,000 nT and vary the dip angle without adjusting the magnitude for latitude.

In all lightning simulations in this paper, we use the modified transmission line method with linear decay (MTLL) lightning return stroke model (see section 4), a return stroke speed of 0.7 c, a terminal altitude of 8 km, a current pulse rise time of $\tau_r = 10$ μs, and a fall time of $\tau_f = 50$ μs. The 3-D FDTD grid uses 1 km grid cells below the ionosphere, transitioning to 500 m grid cells above 70 km altitude. The simulation extends to 250 km range and 110 km altitude, for a full grid that is $156 \times 500 \times 500$ cells. A "full" simulation (with ionosphere and heating) uses 9 GB of computer memory and runs in 14 h on a 12-core processor.

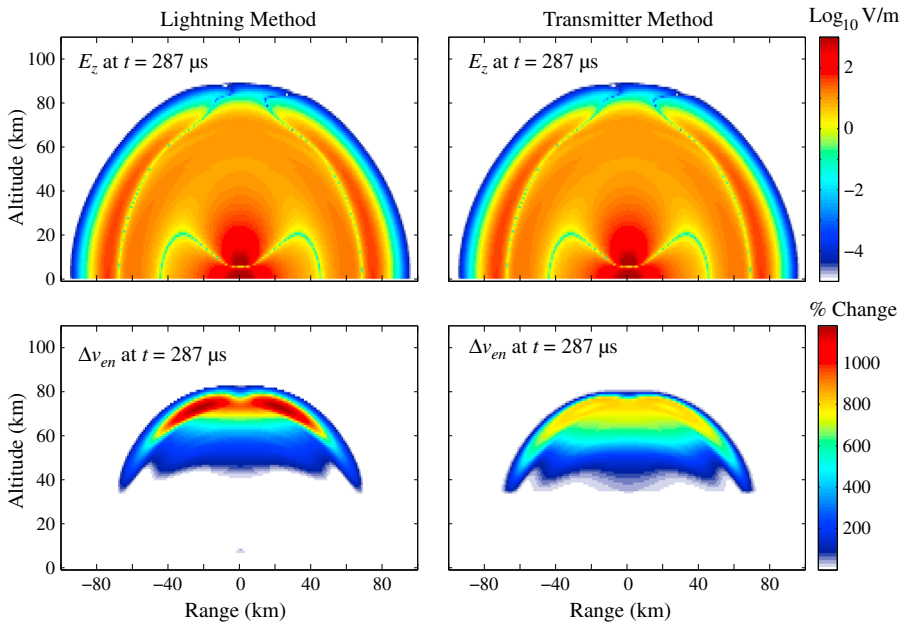

Figure 1. Comparison of heating methods discussed in section 2.1. (top) Snapshot of the vertical electric field at $t = 287$ μs for (left) the lightning heating method and (right) the transmitter method, applied to lightning. (bottom) Percent change in the collision frequency using the two methods applied to the same lightning discharge. Both panels are held to the same color scale to emphasize the relative heating results.

Figure 1 shows a snapshot of the vertical electric field and the modified collision frequency due to a 100 kA lightning discharge; Figure 1 (left) shows E_z and $\Delta\nu_{en}$ using the "lightning" method, and Figure 1 (right) shows the same for the "transmitter" method. The magnetic dip angle is 45° in this case. We choose a relatively early snapshot to compare the two methods; at later times, the transmitter heating method results in an instability due to the rapid increase in electron temperature with the strong lightning fields. Nonetheless, this snapshot shows that $\Delta\nu_{en}$ is qualitatively similar using both methods. Quantitatively, the peak $\Delta\nu_{en}$ is ~1200 % using the lightning method, and ~850 % using the transmitter method, a difference of 30%. This shows that the methods are similar enough to provide accurate, comparable heating results within a few dB.

The difference between the two models can be accounted for by noting that they are fundamentally derived for different heating mechanisms. The lightning method, derived from the Boltzmann equation using BOLSIG+, accounts for the change in electron mobility due to a quasi-steady electric field (steady enough to maintain a stationary electron distribution); thus, the electrons are being heated by adding a well-directed drift velocity. Conversely, the transmitter method accounts for heating through a change in the temperature of the electron distribution through Joule heating; there is no inherent drift component to the electron velocity distribution. Despite this fundamental difference in the approach, the small difference between the two methods shows that the quantitative results of both are physically reasonable.

3. Heating by VLF Transmitters

We begin by investigating the effects of heating by VLF transmitters. In our FDTD model, we use a sinusoidal source at the transmitter frequency, with a peak current that corresponds to the desired transmitter power. The transmitter is modeled as a monopole above the conducting ground; the radiation pattern has been measured in the model and matches the theoretical pattern of a monopole above a conducting surface to within 5%. The relationship between the transmitter radiated power and source current for a small monopole with a triangular current pattern is given by

$$P_{\text{rad}} = \frac{1}{2}\left(\frac{\omega_0^2 h^2}{12\,\pi\epsilon_0 c^3}\right) I_0^2 \tag{3}$$

where $f_0 = \omega_0/2\pi$ is the transmitter frequency, h is the transmitter monopole length, and I_0 is the peak current. For a known transmitter power, we use this to determine the source current to use in the model.

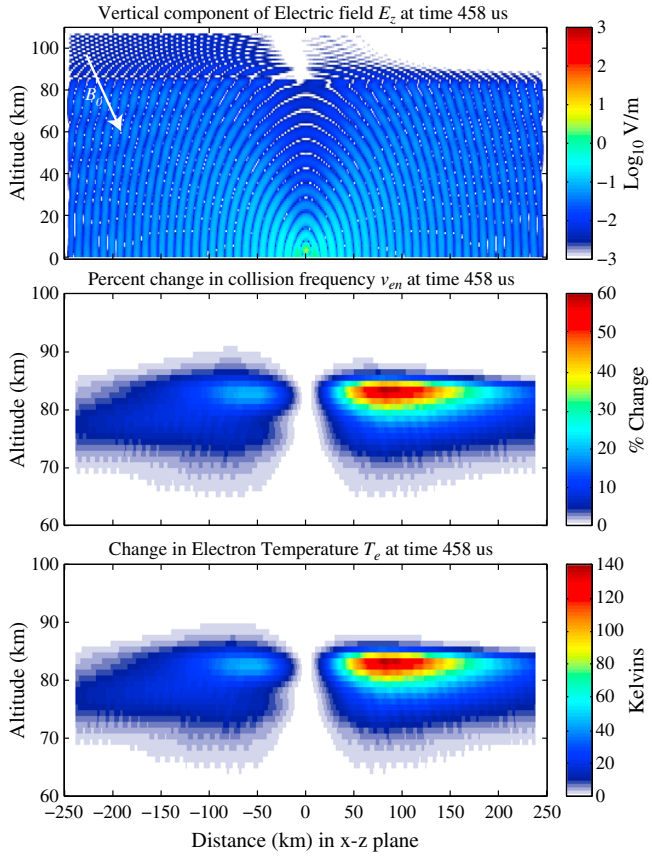

Figure 2. Heating by a 452 kW VLF transmitter, with parameters described in the text. (top) A snapshot of the vertical electric field. (middle) The change in collision frequency due to heating and (bottom) the change in electron temperature.

Each simulation is run three times, under the following conditions: (1) with the ionosphere turned off, i.e. free-space propagation; (2) with the ionosphere turned on, but with no heating effects calculated; and (3) with the ionosphere turned on, and heating and ionization effects turned on.

The ratio of probe fields in simulations 1 and 2 gives the attenuation due to the lower ionosphere, which can be compared to estimates in other work [e.g., *Graf et al.*, 2013a]; the ratio of probe fields in simulations 2 and 3 gives the attenuation strictly due to heating effects. These ratios are what is plotted in most of the figures described in this paper.

Figure 2 shows a 2-D slice of an example simulation. The 452 kW, 21.4 kHz transmitter is located on the ground at $x = 0, z = 0$; this slice is taken in the plane of the magnetic field, which has a 45° dip angle. Figure 2 (top) shows a snapshot of the vertical component of the electric field (E_z); one can clearly observe the ionospheric reflection and resulting mode patterns, as well as stronger transionospheric propagation in the direction parallel to B_0. (Note that the color scale used here is designed to be the same as that of Figure 7, to show the relative amplitude of transmitter and lightning fields.) Figure 2 (middle) shows the change in collision frequency; heating is stronger in the direction propagating across B_0, since the electric field vector is closer to parallel to B_0. Similarly, the electron temperature change ΔT_e, shown in Figure 2 (bottom), is stronger in the direction across B_0. The absolute magnitude of ΔT_e, with a maximum of ~150 K, is in good agreement with *Graf et al.* [2013b], who calculated a maximum $\Delta T_e = 300$ K for the 424 kW NPM transmitter.

Another observation from Figure 2 that is of general interest is the fact that the heating exhibits structure in phase with the propagating sinusoidal wave; peaks and nulls in the heating pattern are evident at half-wavelength intervals. This is not surprising, because the cooling rate is relatively fast compared to the transmitter frequency. The effect is more prominent for lower frequencies for this reason. This shows that the *D* region ionosphere, when heated by VLF transmitters, exhibits structure on scale sizes of a VLF wavelength. These structures may in turn scatter VLF waves from other transmitters, leading to the scattered fields observed by *Graf et al.* [2013a]. These scattered fields are attributed by forward scattering through a very large heated area; but they may in fact be due to wide-angle scattering by a significantly smaller heated area.

3.1. Variation With Transmitter Power

In Figure 3 we investigate the effects of heating on the transmitter signal propagation, as a function of transmitter power. We use a 21.4 kHz transmitter, and a magnetic dip angle of 45° in order to investigate the effects of propagation direction. Figure 3 (left) attempts to show the probe points used; the probe points are spaced in the four cardinal directions, at 50 and 100 km lateral distance from the source. The red and teal points are "along-B_0," and dark blue and yellow points are "across-B_0." In the Northern Hemisphere, then,

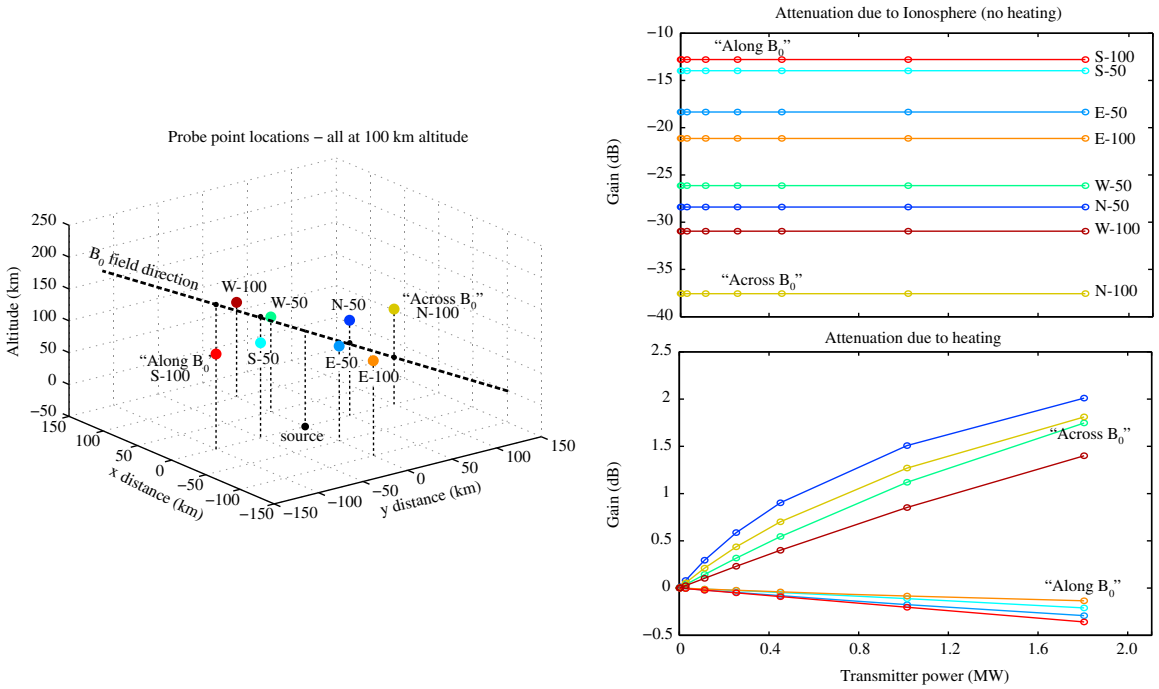

Figure 3. Effects of transmitter heating as a function of transmitter power. (left) Location of probe points with respect to magnetic field. (top right) Gain (negative = attenuation) due the lower ionosphere only, without heating. (bottom right) Gain due to heating, calculated by comparing the heated and unheated cases. The probe point denoted "S-100" refers to the point in the South direction, 100 km from the source, and similarly for the other probe points.

along-B_0 corresponds with south, and across-B_0 is north; brown and green points are west, and light blue and orange points are east. The probe points are denoted "S-100," etc. to clarify their locations in the next few figures.

Figure 3 (top right) shows the attenuation of the transmitter signal due to the lower ionosphere without including heating. We show these ionospheric attenuation results throughout this paper to give a sense of the relative importance of the heating effect compared to the attenuation due to the unheated ionosphere. As expected and observed in Figure 2, propagation across-B_0 is much more strongly attenuated. Propagation in the west direction is also more strongly attenuated than the east direction. There is no dependence on transmitter power, since nonlinear effects have not been included at this point. The magnitude of the attenuation, as well as the variation in North-South and East-West directions, is consistent with modeling and data presented in *Cohen et al.* [2012].

Figure 3 (bottom right) shows attenuation due to the nonlinear heating effects in the lower ionosphere. We observe an initially surprising effect: propagating signals along-B_0 and east are attenuated due to heating by 0−0.5 dB, approximately linear with the transmitter power; but in the directions across-B_0 and west, heating actually provides a net *gain* of up to 2 dB, increasing with transmitter power. This result actually has a simple intuitive explanation, which we will describe in detail in section 5.

3.2. Variation With Dip Angle

Figure 4 shows the effects of heating as a function of magnetic dip angle. All of these runs are for a 452 kW transmitter at 21.4 kHz. A dip angle of zero (left edge of figure) corresponds to a vertical magnetic field, and a dip angle of 90 degrees is a horizontal field, i.e., at the magnetic equator. Note that the values at 90° are prone to error and cannot be trusted; the perfectly matched-layer numerical boundary condition used in the FDTD method is accurate to ~80 dB (i.e., signals are numerically reflected from the boundary with 80 dB attenuation), so a measurement of attenuation of >80 dB is likely to be affected by numerical error from the boundary reflection.

Again, Figure 4 (top left) shows the attenuation due to the lower ionosphere, and Figure 4 (bottom left) shows attenuation due to heating effects. As expected, attenuation due to the lower ionosphere is lowest for

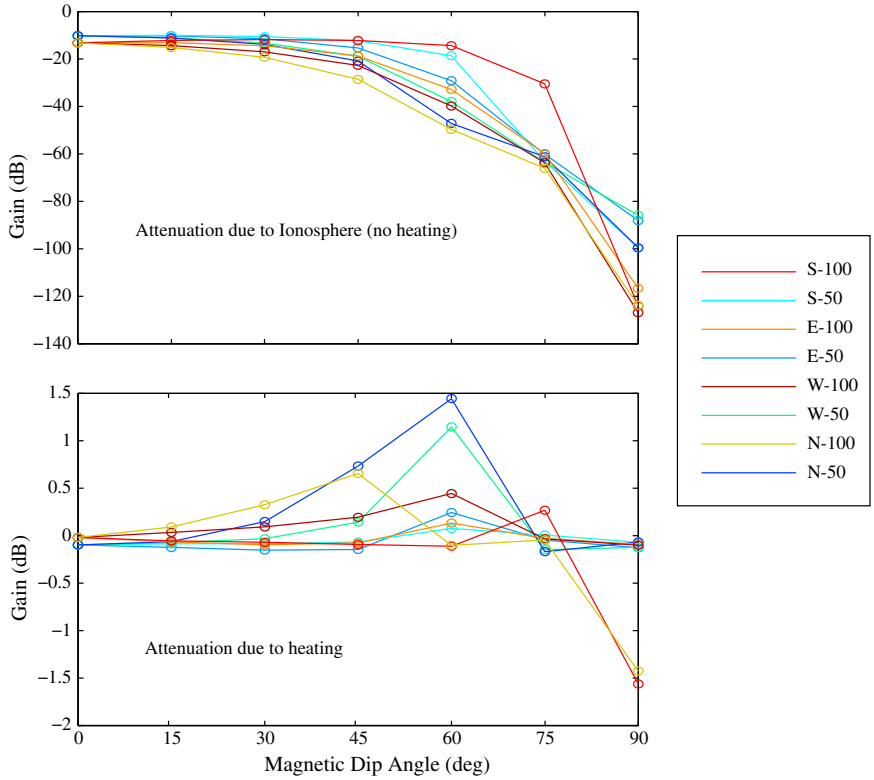

Figure 4. Effects of transmitter heating as a function of magnetic dip angle, i.e., latitude. Colors correspond to the same probe points as in Figure 3 as shown in the legend. The two panels here correspond to Figure 3 (top right) and Figure 3 (bottom right).

a vertical field and is symmetric in the four cardinal directions, varying only with the 50 and 100 km distance. For larger dip angles, all directions have increasing attenuation, but the increase is largest for across-B_0 and west directions (dark blue, yellow, green, and brown).

The trend due to heating is not monotonic and predictable as it is for transmitter frequency; this is because the incidence angle at 50 or 100 km range and 100 km altitude, where the probe points are located, depends on the dip angle; for example, the wave at 100 km range across-B_0 has a 90° incidence angle for a 45° dip angle, but the wave at 50 km range across-B_0 has a nearly 90° incidence angle for a 60° dip angle. Nonetheless, there is a general trend of either small attenuation along-B_0, or up to 1.5 dB gain across-B_0, with variation due to dip angle.

3.3. Variation With Transmitter Frequency

Figure 5 shows the effects of heating as a function of transmitter frequency, using a 45° dip angle and a 500 kW transmitter. The panels and colors follow the same pattern as Figure 4. In Figure 5 (top left), we observe that the attenuation due to the lower ionosphere increases with transmitter frequency, and the effect is strongest in the across-B_0 and west directions. Conversely, in the along-B_0 direction (red), there is almost no variation with the transmitter frequency.

In Figure 5 (bottom left), we observe that in the along-B_0 and east directions, the attenuation due to heating is strongest for lower frequencies, increasing to near zero at 40 kHz. Across-B_0 and west, the heating gain effect increases with transmitter frequency, up to a maximum frequency that depends on the direction, above which the gain decreases again. This effect will also be addressed in section 5.

3.4. U.S. Navy Transmitters

In this section, we look at the attenuation due to heating effects for known VLF transmitters. In particular, we use the power, frequency, and magnetic dip angle at the locations of the NAA, NAU, NPM, NWC, and NLK transmitters operated by the U.S. Navy.

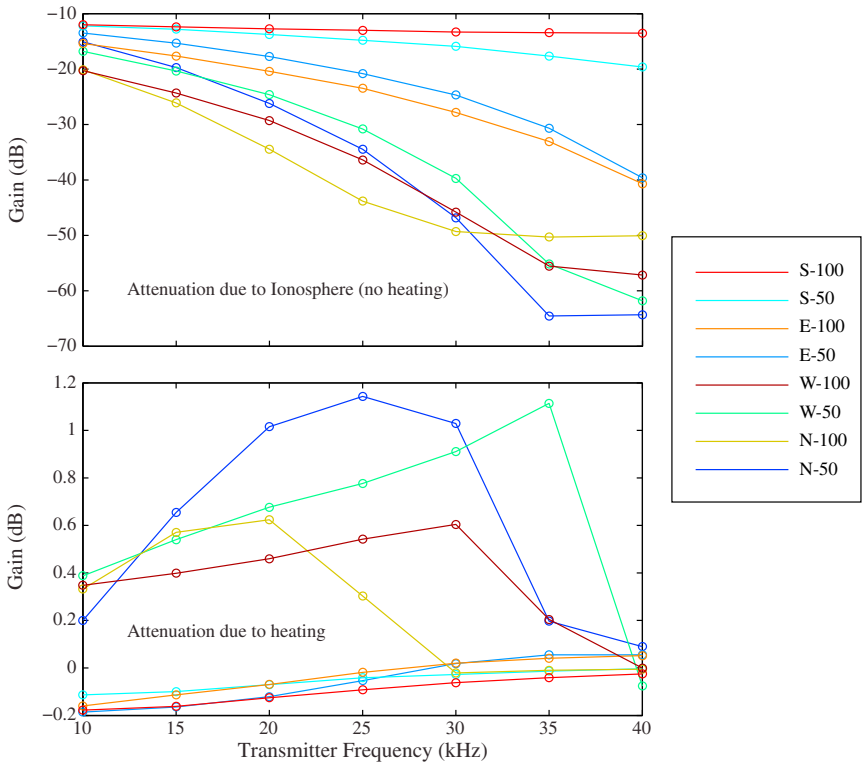

Figure 5. Effects of transmitter heating as a function of transmitter frequency; colors and panels correspond to those in Figure 4.

Figure 6 shows results for the five transmitters, plotted as a function of power; the magnetic dip angle and transmitter powers are noted on the figure. Colored dots indicate the attenuation at each of the probe points; they have been elongated into ellipses in order to identify overlapping dots. NAA and NWC have been moved to the left and right of 1 MW in order to separate them, but they are both simulated with 1 MW transmitted power. We also note that the dot colors appear to flip for NWC, since it's dip angle is negative; the red dot is now "across-B_0," while the yellow dot is "along-B_0 ."

The trends observed earlier can be seen clearly in Figure 6 (top panel): The ionospheric attenuation for NLK and NAA are nearly identical due to their very similar dip angle, and the attenuation does not depend on power. Attenuation is greatest for the transmitters with higher dip angles, i.e., closer to the equator. For attenuation due to heating, in Figure 6 (bottom panel), the general trend of higher attenuation or gain with higher transmitter power is evident, and the attenuation/gain trends with propagation direction are evident as well. NPM has slightly anomalously high heating gain for its transmitter power; this is likely due to the high dip angle, providing near-45° incident angle for the dark blue and yellow probe points. Overall, each of the transmitters exhibits 0–0.7 dB of attenuation or gain, depending on the propagation direction.

We can conclude from this result that for VLF transmitters, the attenuation due to heating is a small effect, likely smaller than other known uncertainties which lead to the ~6 dB discrepancy between observations and model results.

4. Heating by Lightning

Since the publication of *Marshall* [2012], we have added a key feature to the EMP lightning model, which is the ability to accurately model the lightning return stroke using known engineering models. We have incorporated the spatiotemporal evolution of the lightning return stroke using seven known models (summarized in *Rakov and Uman* [2003]), which can be selected at runtime: (1) Bruce-Golde method [*Bruce and Golde*, 1941], (2) transmission line method (TL) [*Uman*, 1969], (3) modified transmission line method with linear decay (MTLL) [*Rakov and Dulzon*, 1987], (4) modified transmission line method with exponential

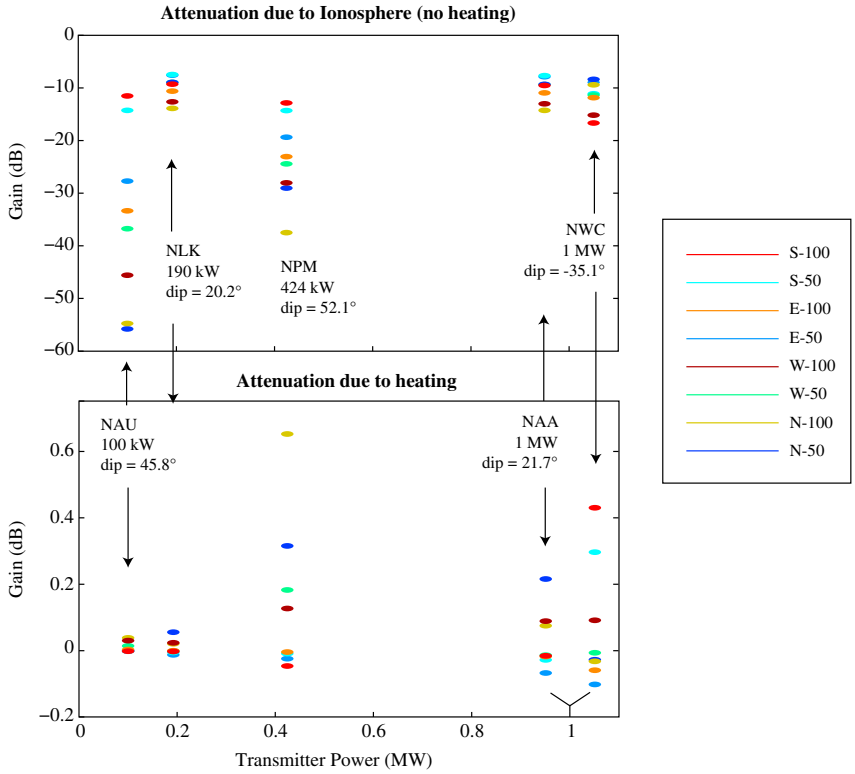

Figure 6. Effects of transmitter heating for known U.S. Navy transmitters.

decay [*Nucci et al.*, 1988], (5) traveling current source method [*Heidler*, 1985], and (6) Diendorfer and Uman method [*Diendorfer and Uman*, 1990].

The seventh method is a "dummy" method, essentially the TL method with infinite return stroke speed. In all simulations in this paper, we use the MTLL method, with return stroke speed $v_{rs} = 0.7\,c$, 10 μs rise time, 50 μs fall time, and 8 km terminal altitude. The lightning current as a function of time on the ground is given by equation (5) in *Marshall* [2012].

We have run validation tests of the EMP model using the TL return stroke model to compare to measurements. At a distance of 100 km, with a return-stroke speed of $\frac{1}{2}c$, *Orville* [1991] show that the peak current I_0 is related to the measured electric field E_{100} (accounting for the distance delay) by $I_0 \simeq 3.3\,E_{100}$, with I_0 in kA and E_{100} in V/m. Using a lightning channel length of 5 km, measuring the electric field at 100 km from the source, we find the relationship in the EMP model to be $I_0 = 3.54\,E_{100}$, very close to the result in *Orville* [1991].

Figure 7 shows a 2-D slice of an example lightning simulation. The lightning discharge is located on the ground at the center of the simulation space; again, this slice is taken in the plane of the magnetic field, which has a 45° dip angle. Figure 7 (top) shows a snapshot of the vertical component of the electric field (E_z); one can clearly observe the EMP, the lightning QE field, the ionospheric reflection, and whistlers propagating through the ionosphere. Figure 7 (middle) shows the change in collision frequency; Figure 7 (bottom) shows the change in electron density due to attachment. In this case, the electron density change is purely negative due to dissociative attachment, implying that the effective electric field E_{eff} never exceeded the breakdown field E_k.

It is important to note that the measurement of ionospheric attenuation is not entirely accurate, because it only includes attenuation up to the probe point altitude of 100 km. Any attenuation or dispersion due to the ionosphere above 100 km is not included. However, using a 2-D version of the model, we can estimate the heating that occurs above and below 100 km. We run a 2-D simulation up to 250 km altitude; this requires a much smaller grid cell and time step, which would result in a simulation time of many days for the 3-D model. We calculate Joule heating in the model at each time step and integrate in time to find the

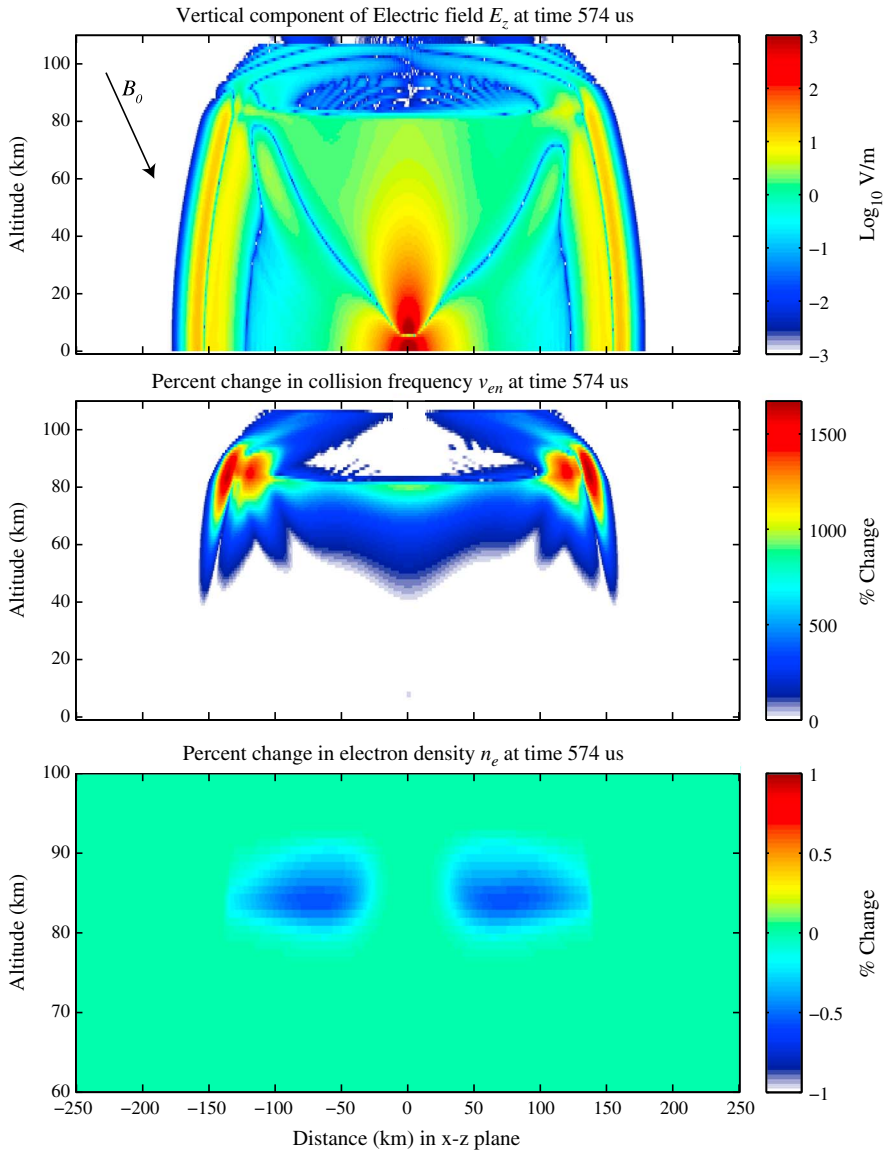

Figure 7. Heating by a 100 kA lightning discharge, with parameters described in the text. (top) A snapshot of the vertical electric field. (middle) The change in collision frequency due to heating and (bottom) the change in electron density due to detachment, attachment, and ionization.

energy lost due to heating. The 2-D simulation of a 100 kA discharge shows that 99.2% of the heating occurs below 100 km altitude. This is reflected in Figures 2 and 7 (bottom), where we observe that the changes in collision frequency, temperature, and electron density are well confined below 100 km altitude. (In Figure 7, middle, we plot the percent change in collision frequency; but the collision frequency decreases exponentially with altitude, so the absolute $\Delta\nu_e$ is very small above 100 km.) This analysis shows that the attenuation calculations in this paper are a very close approximation to the total attenuation through the ionosphere.

4.1. Variation With Peak Current

Figure 8 shows results for a series of simulations where the peak current is varied from less than 1 kA up to 300 kA. Figure 8 (top, left) shows the locations of probe points; here we have increased the number of probe points to 21, including five in each of the cardinal directions, from 20 to 100 km range, and one directly above the lightning discharge. Crucially, the red probe point is in the direction along-B_0 and the orange probe point is in the direction across-B_0. Figure 8 (bottom, left) shows attenuation due to the lower ionosphere without heating; this attenuation is determined from the peak of the sferic or whistler as it

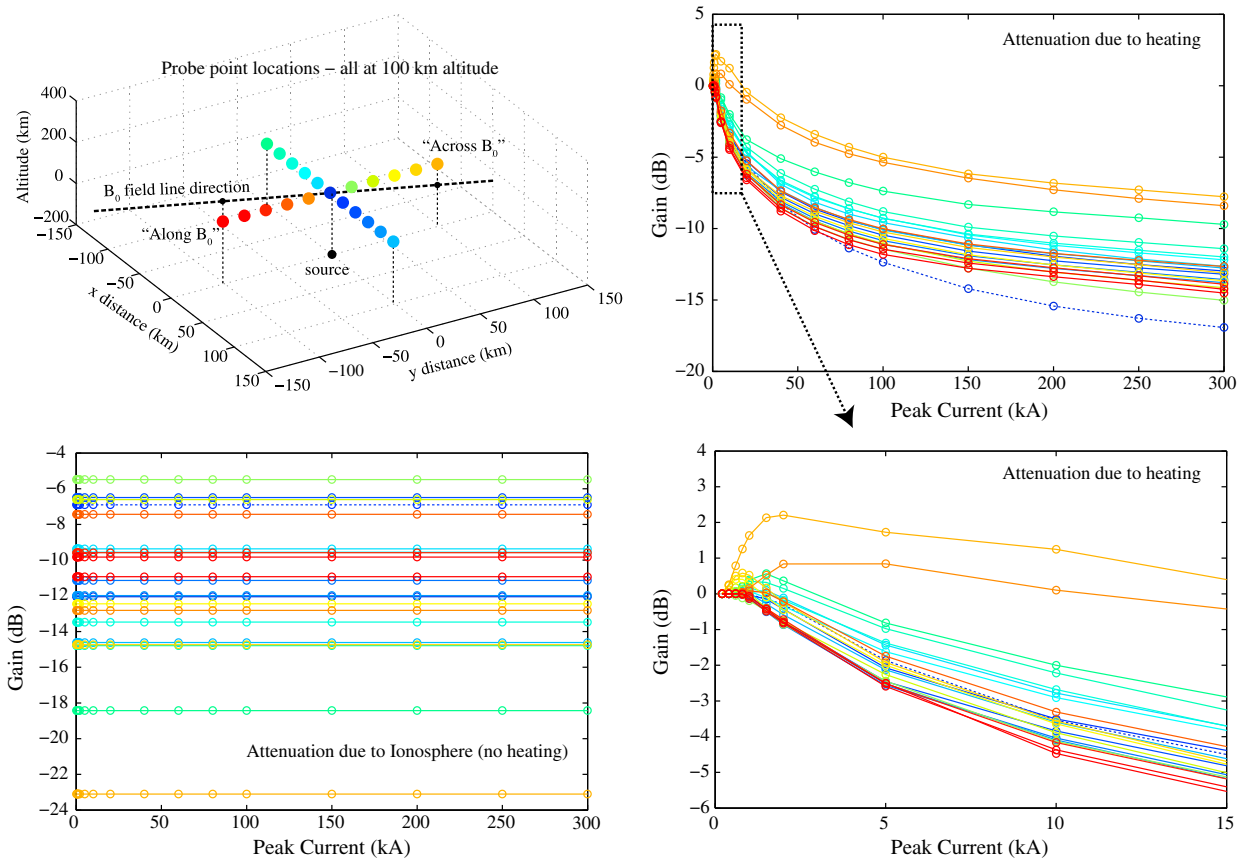

Figure 8. Effects of lightning heating as a function of peak current. (top, left) Probe points used. (bottom, left) Gain due to the lower ionosphere without heating. Note that probe point directly above the lightning discharge is denoted with a dashed line. (top, right) Gain due to heating and ionization. (bottom, right) Zoom in to small peak current range.

propagates past the probe points. Clearly, the attenuation is independent of peak current, since nonlinear effects have not been included.

Figure 8 (right) shows the attenuation due to heating; Figure 8 (bottom, right) is a zoomed-in view of Figure 8 (top, right) over the range from 0 to 15 kA. As expected, we see attenuation increasing (gain decreasing) with increasing peak current for all probe points; the effect of heating is strongest for along-B_0 and east directions, and weaker for across-B_0 and west directions. We also observe that the directions across-B_0 and west exhibit a small "gain" for low peak currents, similar to the VLF transmitter results in Figure 3. The gain reaches a maximum of only 2 dB before the curve turns over, and above 15 kA, all probe points exhibit attenuation. We provide discussion and interpretation of these results in section 5.

The most important observation, of course, is that the attenuation due to heating is as high as a few dB even for lighting below 10 kA, and as high as 10 dB or more for large discharges. Clearly this shows that the effect of heating must be taken into account for an accurate assessment of ionospheric absorption of lightning-induced VLF signals.

4.2. Variation With Dip Angle

In Figure 9 we investigate the effects of heating over the range of magnetic dip angles from 0° (vertical B_0) to 75°. We have excluded the results at 90° dip angle for the reasons described in section 3.2, namely because the attenuation is larger than the numerical accuracy of the model. This problem occurs for a 75° dip angle for the across-B_0 orange probe point, which explains its unusual behavior for a 75° dip angle.

The simulations shown in Figure 9 use a 100 kA lightning discharge and the standard IRI ionosphere. As expected, for all probe points except one, the attenuation due to the lower ionosphere increases (gain decreases) with dip angle, with some irregularities due to the incidence angle effect described in section 3.2. The exception is the dark blue curve, which is the probe point directly above the source. Here the gain

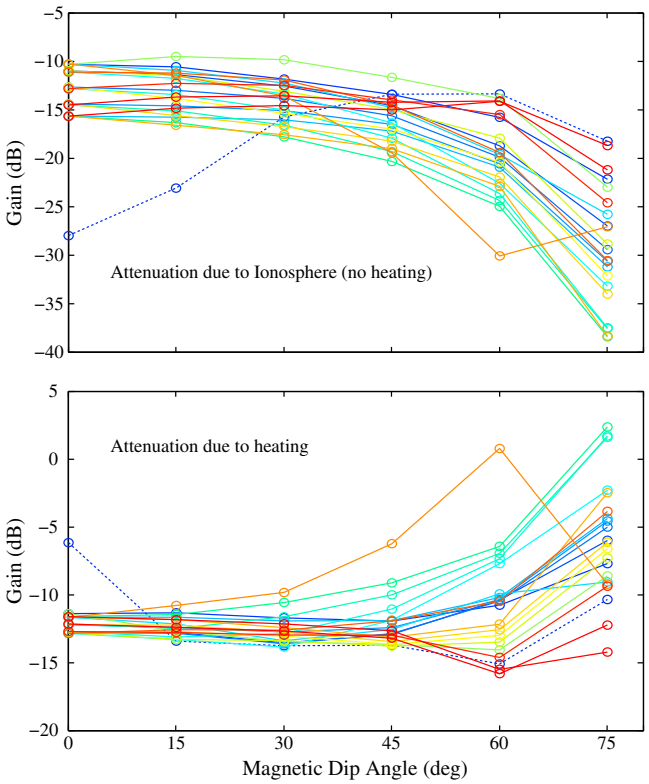

Figure 9. Effects of lightning heating as a function of magnetic dip angle, i.e., latitude. The colors correspond to the probe points in Figure 8. (top) Gain due to the lower ionosphere without heating and (bottom) gain due to heating and ionization. Results are unreliable at 90° dip angle (i.e., equatorial) due to numerical boundary issues in the model.

increases with dip angle, up to 60° dip angle, due to refraction effects.

In Figure 9 (bottom), the attenuation due to heating is maximum (gain minimum) for the vertical field, and generally decreases (gain increases) with increasing dip angle. The heating effect appears to be a weak function of dip angle for near-vertical fields (0–45° dip angle), with a more direction-dependent effect at higher dip angles (more horizontal fields).

4.3. Variation With Ionosphere Density

Finally, we investigate the effects of ionospheric density on attenuation in Figure 10. As shown in Figure 10 (left), we modify the IRI ionosphere profile used throughout this work by multiplying by a constant factor from 0.2 to 5; this follows the method of *Cohen et al.* [2012]. Figure 10 (top right) shows the attenuation due to the lower ionosphere without heating; the colors represent the probe points in Figure 8. As expected, the general trend is that attenuation increases with ionospheric density and is highest for the across-B_0 directions.

In Figure 10 (bottom right) we show the attenuation due to heating. The effect appears to increase (decreasing gain) with ionospheric density for all probe points, up to about 1 × IRI density; above that the effect either remains constant for some probe points, or even begins to decrease, in particular for the across-B_0 probe points (orange).

5. Summary and Discussion

We have presented simulations of VLF transmitter and lightning EMP signal propagation through the *D* region ionosphere and used these to estimate the attenuation or gain of the signal due to the nonlinear heating effects of the wave on the ionosphere. Our key results can be summarized as follows:

1. For VLF transmitters with transmitted power up to 2 MW, self-consistent heating affects the transionospheric propagation of the transmitter signal by up to ~1 dB.
2. Depending on the propagation direction, the signal can either be further attenuated by heating, by up to ~0.5 dB, or can be enhanced by heating by up to ~1 dB.
3. For lightning, self-consistent heating of the *D* region ionosphere affects the transionospheric propagation by up to 10 dB or more; the attenuation monotonically increases with lightning peak current above 15 kA.
4. For low peak currents below 15 kA, the lightning energy can be enhanced by heating by up to 1–2 dB, similar to the effect observed for VLF transmitters.
5. Attenuation due to heating is generally higher for low magnetic dip angles (i.e., vertical B_0).
6. Attenuation due to heating is generally higher for a more dense ionosphere, up to about 1–2 times the baseline IRI ionosphere profile. For more dense profiles the heating effect appears to saturate.

As briefly noted earlier, a surprising effect is evident in the direction across-B_0 and west, observed in Figures 3 and 8. Particularly for low amplitudes (VLF transmitters and low peak current lightning), the effect

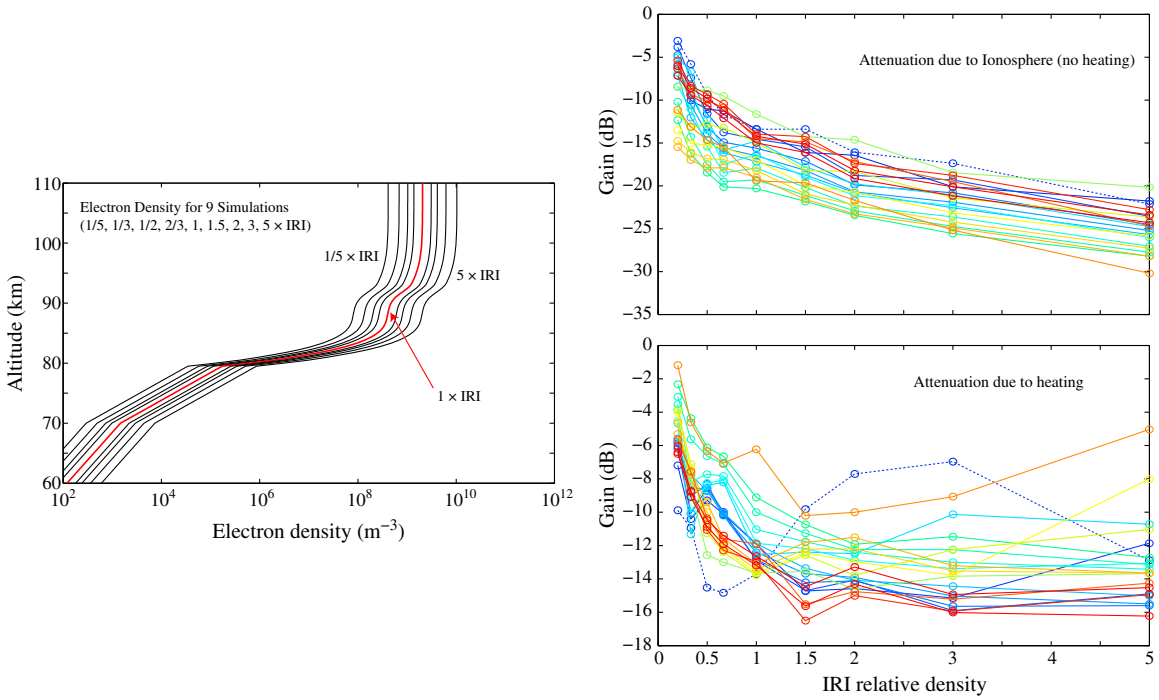

Figure 10. Effects of lightning heating with different ionosphere profiles. The colors correspond to the probe points in Figure 8. (left) The profiles used, which are the IRI profile scaled by the factors in the legend. (right) Panels correspond to those in Figure 9.

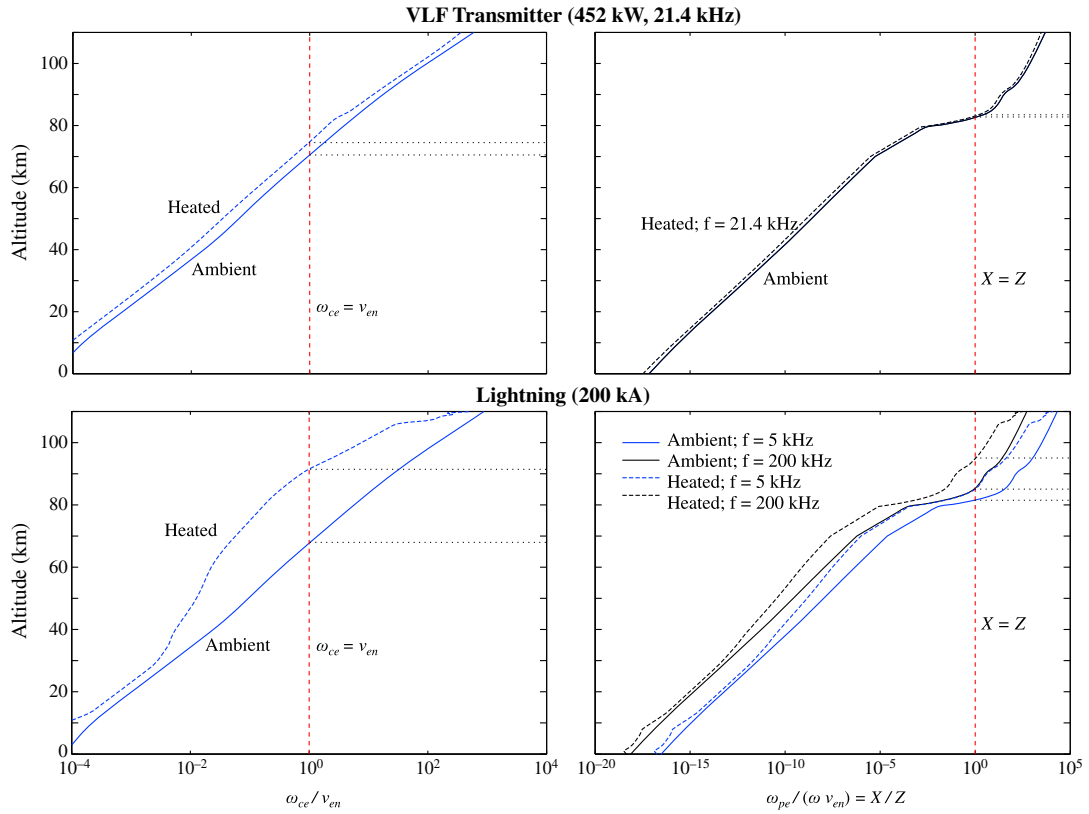

Figure 11. Effects of ionospheric heating. (top) Effects by a 452 kW VLF transmitter at 21.4 kHz; (bottom) effects of a 200 kA lightning discharge, with other parameters as described in the text. (left) The ratio of gyrofrequency ω_{ce} to collision frequency ν_{en}; (right) the ratio X/Z. Dashed lines show the effects of heating, compared to the ambient (solid) ionosphere.

of heating actually allows more energy to propagate through the ionosphere, leading to an observed gain relative to the no-heating cases.

We interpret this effect with reference to Figure 11. Here we calculate the ratio of the gyrofrequency to the electron-neutral collision frequency ω_{ce}/ν_{en} in Figure 11 (left), and the ratio X/Z in Figure 11 (right), where $X = \omega_{pe}^2/\omega^2$ and $Z = \nu_{en}/\omega$ from the magneto-ionic theory. Figure 11 (top) is for a 452 kW VLF transmitter at 21.4 kH, and Figure 11 (bottom) for a 200 kA lightning discharge. In both cases we find the maximum change in ν_{en} and N_e at each altitude (the latter of which affects ω_{pe}).

The ratio ω_{ce}/ν_{en} measures the extent of magnetization of the plasma. When $\omega_{ce}/\nu_{en} \ll 1$, the plasma is so collisional that it is essentially unmagnetized; electrons cannot make even a fraction of a gyration before colliding with a neutral particle. When $\omega_{ce}/\nu_{en} \gg 1$, the plasma is completely magnetized, and waves cannot propagate across B_0. In Figure 11 (right), the altitude at which $X = Z$ gives the reflection altitude for a particular frequency; here we plot X/Z for VLF frequencies of 5 and 200 kHz in order to roughly bound the energy in the lightning radiated field.

These four plots show that when the ionosphere is heated, either by a VLF transmitter or by lightning, (a) the altitude of VLF reflection increases and (b) the magnetization altitude (where $\omega_{ce} > \nu_{en}$) increases. These effects imply respectively that (a) more energy reaches higher altitudes before reflection and (b) waves reach higher altitude before encountering the "magnetized" ionosphere. In the direction along-B_0, the latter (b) has little effect, since the wave can freely propagate along B_0; but in the direction across-B_0, the wave is able to propagate to higher altitudes before encountering the hindering effect of the perpendicular magnetic field. It is this effect that we believe accounts for the gain in the signal for low amplitudes. For higher amplitudes (>15 kA lightning), the fundamental effect of absorption due to the $\nu_{en}J$ term in the Lorentz equation becomes so large as to dominate.

Acknowledgments

This work was supported by NSF CEDAR/GEM Postdoctoral Fellowship AGS-1027070 and NSF CEDAR grant AGS-1243176. The EMP model and analysis codes used to produce the results in this paper are available upon request from the author.

Alan Rodger thanks Janusz Mlynarczyk and an anonymous reviewer for their assistance in evaluating this paper.

References

Abel, B., and R. M. Thorne (1998), Electron scattering in the Earth's inner magnetosphere: 1. Dominant physical processes, *J. Geophys. Res.*, *103*, 2385–2396.

Banks, P. (1966), Collision frequencies and energy transfer: Electrons, *Planet. Space Sci.*, *14*, 1085–1103.

Bilitza, D., and B. Reinisch (2008), International reference ionosphere 2007: Improvements and new parameters, *J. Adv. Space Res.*, *42*(4), 599–609, doi:10.1016/j.asr.2007.07.048.

Bortnik, J. (2004), Precipitation of radiation belt electrons by lightning-generated magnetospherically reflecting whistler waves, PhD thesis, Stanford Univ., Palo Alto, Calif.

Bruce, C. E. R., and R. H. Golde (1941), The lightning discharge, *J. Inst. Electron. Eng.*, *88*, 487–520.

Cho, M., and M. J. Rycroft (2001), Non-uniform ionisation of the upper atmosphere due to the electromagnetic pulse from a horizontal lightning discharge, *J. Atmos. Sol. Terr. Phys.*, *63*, 559–580.

Cohen, M. B., and U. S. Inan (2012), Terrestrial VLF transmitter injection into the magnetosphere, *J. Geophys. Res.*, *117*, A08310, doi:10.1029/2012JA017992.

Cohen, M. B., N. G. Lehtinen, and U. S. Inan (2012), Models of ionospheric VLF absorption of powerful ground based transmitters, *Geophys. Res. Lett.*, *39*, L24101, doi:10.1029/2012GL054437.

Diendorfer, G., and M. A. Uman (1990), An improved return stroke model with specified channel-base current, *J. Geophys. Res.*, *95*(D9), 13,621–13,644.

Glukhov, V. S., and U. S. Inan (1996), Particle simulation of the time-dependent interaction with the ionosphere of rapidly varying lightning EMP, *Geophys. Res. Lett.*, *23*(16), 2193–2196.

Golden, D. I., M. Spasojevic, F. R. Foust, N. G. Lehtinen, N. P. Meredith, and U. S. Inan (2010), Role of the plasmapause in dictating the ground accessibility of ELF/VLF chorus, *J. Geophys Res.*, *115*, A11211, doi:10.1029/2010JA015955.

Graf, K. L., N. G. Lehtinen, M. Spasojevic, M. B. Cohen, R. A. Marshall, and U. S. Inan (2013a), Analysis of experimentally-validated trans-ionospheric attenuation estimates of VLF signals, *J. Geophys. Res. Space Physics*, *118*, 2708–2720, doi:10.1002/jgra.50228.

Graf, K. L., M. Spasojevic, R. A. Marshall, N. G. Lehtinen, F. R. Foust, and U. S. Inan (2013b), Extended lateral heating of the nighttime ionosphere by ground-based VLF transmitters, *J. Geophys. Res. Space Physics*, *118*, 7783–7797, doi:10.1002/2013JA019337.

Hagelaar, G. J. M., and L. C. Pitchford (2005), Solving the Boltzmann equation to obtain electron transport coefficients and rate coefficients for fluid models, *Plasma Sources Sci. Technol.*, *14*, 722–733.

Hedin, A. E. (1991), Extension of the MSIS thermospheric model into the middle and lower atmosphere, *J. Geophys Res.*, *96*, 1159–1172.

Heidler, F. (1985), Traveling current source model for LEMP calculation, paper presented at the 6th International Symposium on Electromagnetic Compatibility, pp. 157–162, Swiss Fed. Inst. of Technol., Zurich, Switzerland.

Helliwell, R. A. (1965), *Whistlers and Related Ionospheric Phenomena*, Stanford Univ. Press, Stanford, Calif.

Imhof, W. L., J. B. Reagan, H. D. Voss, E. E. Gaines, D. W. Datlowe, J. Mobilia, R. A. Helliwell, U. S. Inan, J. P. Katsufrakis, and R. G. Joiner (1983), Direct observation of radiation belt electrons precipitated by the controlled injection of VLF signals from a ground-based transmitter, *Geophys. Res. Lett.*, *10*, 361–364.

Inan, U. S., and D. L. Carpenter (1987), Lightning-induced electron precipitation events observed at L=2.4 as phase and amplitude perturbations on subionospheric VLF signals, *J. Geophys. Res.*, *92*(A4), 3293–3303.

Kulkarni, P., U. S. Inan, T. F. Bell, and J. Bortnik (2008), Precipitation signatures of ground-based VLF transmitters, *J. Geophys. Res.*, *113*, A07214, doi:10.1029/2007JA012569.

Lee, J. H., and D. Kalluri (1999), Three-dimensional FDTD simulation of electromagnetic wave transformation in a dynamic inhomogeneous magnetized plasma, *IEEE Trans. Ant. Prop.*, *47*(7), 1146–1151.

Lehtinen, N. G., and U. S. Inan (2008), Radiation of ELF/VLF waves by harmonically varying currents into a stratified ionosphere with application to radiation by a modulated electrojet, *J. Geophys Res.*, *113*, A06301, doi:10.1029/2007JA012911.

Lehtinen, N. G., and U. S. Inan (2009), Full-wave modeling of transionospheric propagation of VLF waves, *Geophys. Res. Lett.*, *36*, L03104, doi:10.1029/2008GL036535.

Liu, N. (2011), Multiple ion species fluid modeling of sprite halos, paper presented at 30th URSI General Assembly and Scientific Symposium, Istanbul, Turkey.

Luque, A., and F. J. Gordillo-Vázquez (2011), Mesospheric electric breakdown and delayed sprite ignition caused by electron detachment, *Nat. Geosci.*, *5*, 22–25.

Marshall, R. A. (2012), An improved model of the lightning electromagnetic field interaction with the D-region ionosphere, *J. Geophys Res.*, *117*, A03316, doi:10.1029/2011JA017408.

Marshall, R. A., U. S. Inan, and V. S. Glukhov (2010), Elves and associated electron density changes due to cloud-to-ground and in-cloud lightning discharges, *J. Geophys. Res.*, *115*, A00E17, doi:10.1029/2009JA014469.

Nagano, I., S. Yagitani, K. Miyamura, and S. Makino (2003), Full-wave analysis of elves created by lightning-generated electromagnetic pulses, *J. Atmos. Sol. Terr. Phys.*, *65*(5), 615–625.

Neubert, T., O. Chanrion, E. Arnone, F. Zanotti, S. Cummer, J. Li, M. Füllekrug, S. Soula, and O. van der Velde (2011), The properties of a gigantic jet reflected in a simultaneous sprite: Observations interpreted by a model, *J. Geophys Res.*, *116*, A12329, doi:10.1029/2011JA016928.

Nucci, C. A., C. Mazzetti, F. Rachidi, and M. Ianoz (1988), On lightning return stroke modesl for LEMP calculations, paper presented at 19th International Conference on Lightning Protection, pp. 463–469, Assoc. of Aust. Electr. Eng. (OVE), Graz, Austria.

Orville, R. E. (1991), Calibration of a magnetic direction finding network using measured triggered lightning return stroke peak currents, *J. Geophys. Res.*, *96*, 17,135–17,142.

Pasko, V. P., U. S. Inan, T. F. Bell, and Y. N. Taranenko (1997), Sprites produced by quasi-electrostatic heating and ionization in the lower ionosphere, *J. Geophys. Res.*, *102*(A3), 4529–4561.

Rakov, V. A., and A. A. Dulzon (1987), Calculated electromagnetic fields of lightning return stroke, *Tekh. Elektrodinam.*, *1*, 87–89.

Rakov, V. A., and M. A. Uman (2003), *Lightning: Physics and Effects*, Cambridge Univ. Press, Cambridge, U. K.

Rodriguez, J., U. S. Inan, and T. F. Bell (1994), Heating of the nighttime D region by very low frequency transmitters, *J. Geophys. Res.*, *99*(A12), 23,329–23,338.

Rodriguez, J. V. (1994), Modification of the earth's ionosphere by very-low-frequency transmitters, PhD thesis, Stanford Univ., Stanford, Calif.

Starks, M. J., R. A. Quinn, G. P. Ginet, J. M. Albert, G. S. Sales, B. W. Reinisch, and P. Song (2008), Illumination of the plasmasphere by terrestrial very low frequency transmitters: Model validation, *J. Geophys Res.*, *113*, A09320, doi:10.1029/2008JA013112.

Taranenko, Y. N., U. S. Inan, and T. F. Bell (1993a), The interaction with the lower ionosphere of electromagnetic pulses from lightning: Heating, attachment, and ionization, *Geophys. Res. Lett.*, *20*(15), 1539–1542.

Taranenko, Y. N., U. S. Inan, and T. F. Bell (1993b), The interaction with the lower ionosphere of electromagnetic pulses from lightning: Excitation of optical emissions, *Geophys. Res. Lett.*, *20*(23), 2675–2678.

Uman, M. A. (1969), *Lightning*, McGraw-Hill, New York.